

## Variability of fCO<sub>2</sub> in the Eastern Tropical Atlantic from a moored buoy

Nathalie Lefèvre,<sup>1</sup> Antoine Guillot,<sup>2</sup> Laurence Beaumont,<sup>3</sup> and Théo Danguy<sup>3</sup>

Received 6 February 2007; revised 21 September 2007; accepted 9 November 2007; published 23 January 2008.

[1] A fCO<sub>2</sub> sensor, based on a colorimetric method used for the CARIOCA buoys, has been installed on a Pilot Research Moored Array in the Tropical Atlantic (PIRATA) mooring at 6°S, 10°W, in the gulf of Guinea, in June 2006 during the EGEE 3 cruise. Hourly fCO<sub>2</sub> data recorded from June to December 2006 are presented. An alkalinity-salinity relationship has been determined using data from different cruises, which allows the calculation of dissolved inorganic carbon. Although the tropical Atlantic is an important source of CO<sub>2</sub>, an unexpected area of low CO<sub>2</sub> concentrations is observed in the South Equatorial Counter Current with fCO<sub>2</sub> values close to equilibrium conditions or even slightly undersaturated with respect to the atmospheric fCO<sub>2</sub> value of 367.7 μatm measured during the cruise. At the end of June, an increase of seawater fCO<sub>2</sub> to 400 μatm is consistent with the beginning of the upwelling season occurring from July to September. Although the mooring is not located within the upwelling area, the spreading of the cold tongue explains the large CO<sub>2</sub> outgassing. The monthly CO<sub>2</sub> flux ranges from 1.19 mmol m<sup>-2</sup> d<sup>-1</sup> in June to a maximum of 8.37 mmol m<sup>-2</sup> d<sup>-1</sup> in October, when high fCO<sub>2</sub> values above 420 μatm are maintained by the warming of surface water. Most of the fCO<sub>2</sub> distribution can be explained by physical processes and a strong relationship between fCO<sub>2</sub> and SST is determined for the upwelling season. From mid-September, diurnal cycles can be detected. Using a dissolved inorganic carbon budget, periods where net community production or diurnal warming and cooling dominates are observed.

**Citation:** Lefèvre, N., A. Guillot, L. Beaumont, and T. Danguy (2008), Variability of fCO<sub>2</sub> in the Eastern Tropical Atlantic from a moored buoy, *J. Geophys. Res.*, 113, C01015, doi:10.1029/2007JC004146.

### 1. Introduction

[3] The tropical Atlantic is the second most intense oceanic source of CO<sub>2</sub> for the atmosphere after the equatorial Pacific. Although several cruises have sampled the region, the estimate of the CO<sub>2</sub> flux and its spatial and temporal variability are not well determined yet. Each year, in spring-summer an important equatorial upwelling develops in the eastern part of the Atlantic, bringing cold and CO<sub>2</sub>-rich waters to the surface. As these waters warm up westward, the fugacity of CO<sub>2</sub> (fCO<sub>2</sub>) increases in the ocean leading to an increasing outgassing of CO<sub>2</sub> that is stronger in July than in January [Andrié *et al.*, 1986; Oudot *et al.*, 1995]. The thermocline is shallower in the eastern part of the basin, and seasonal variations of sea surface temperature (SST) are greater in the Gulf of Guinea than in the western tropical Atlantic [Merle, 1980]. The Gulf of Guinea is of particular importance as this region is also subject to coastal upwellings. In the northern hemisphere a seasonal coastal upwelling develops between Cape Palmas (Ivory Coast) and Cape three points (Ghana) and Cotonou (Benin) driving the

biology of the system [Hardman-Mountford and McGlade, 2003] and in the southern hemisphere a coastal upwelling takes place between Gabon and Angola. The major upwelling season occurs between July and September. Along the coasts of Gabon and Angola, the upwelling spreads westward by the advection of the South Equatorial Current (SEC) or the effects of Rossby waves propagation to merge with the equatorial upwelling [Ajao and Houghton, 1998] from July to September. Therefore the magnitude of the tropical source of CO<sub>2</sub> will likely depend on the strength of the upwellings. Rivers, such as the Congo, might also affect the surface CO<sub>2</sub> concentration.

[4] In addition to the seasonal variability, the tropical Atlantic exhibits an interannual variability evidenced by warm events sometimes referred to as Atlantic El Niño [Hisard, 1980]. They are indeed similar to the Pacific El Niño as they are characterized by a weakening of the trade winds, and hence a decrease of the equatorial upwelling.

[5] The equatorial circulation is very dynamic and short term variations are missed by the coarse time and space scale of research cruises. To document and understand the CO<sub>2</sub> distribution in the tropical Atlantic, it is necessary to monitor the CO<sub>2</sub> variability in the upper ocean. In this context, a CO<sub>2</sub> observational network is being set up as part of the European project CARBOOCEAN. Time-series stations provide a useful means to document the dynamics of the ocean circulation and the seasonal evolution of the

<sup>1</sup>IRD LOCEAN, Université Pierre et Marie Curie, Paris, France.

<sup>2</sup>DT INSU, Bâtiment Institut Polaire, Plouzané, France.

<sup>3</sup>DT INSU, Meudon, France.

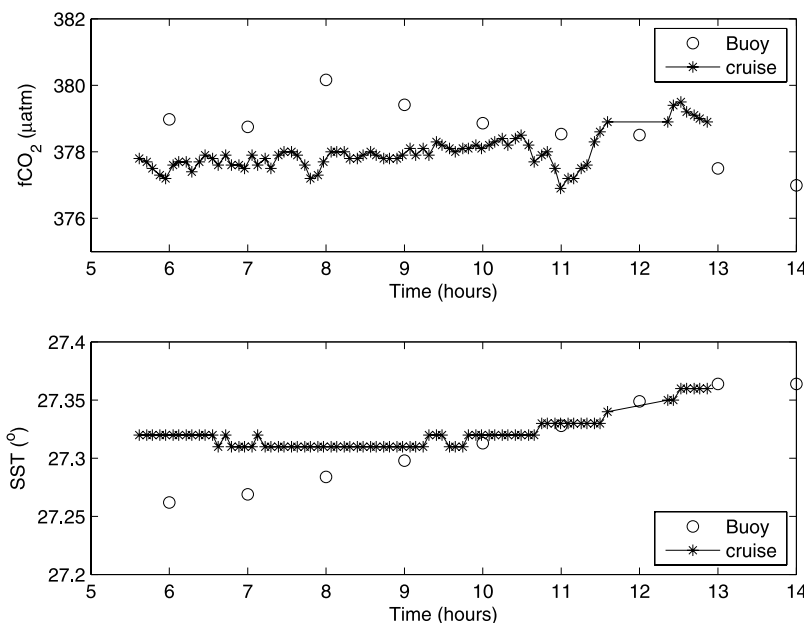


**Figure 1.** Comparison of SST and fCO<sub>2</sub> between the CO<sub>2</sub> sensor (colorimetric method) and the underway system (infrared detection) on the 7th of June 2006.

fugacity of CO<sub>2</sub>. Thus the Hawaiian Ocean Time-series, HOT [Winn *et al.*, 1998], the Bermuda Atlantic Time-series, BATS [Bates, 2001] and the European Station for Time series in the Ocean at the Canary islands, ESTOC [e.g., González Dávila *et al.*, 2003] provide long-term records of CO<sub>2</sub>. However, these stations require significant ship time to provide monthly monitoring of the CO<sub>2</sub> properties. The technological development of small autonomous in situ CO<sub>2</sub> sensors has led to a new generation of time-series. For example, in the tropical Pacific, some Tropical Atmosphere Ocean (TAO) moorings are now equipped with infrared CO<sub>2</sub> instruments [Chavez *et al.*, 1999] and in the Baltic Sea a SAMI-CO<sub>2</sub> sensor [DeGrandpre *et al.*, 1995] was installed on a moored platform [Kuss *et al.*, 2006] but high frequency measurements are still scarce. In the tropical Atlantic, a program called PIRATA (Pilot Research Moored Array in the Tropical Atlantic) has been set up with the main purpose of studying the ocean-atmosphere interactions that are relevant to regional climate variability on a seasonal, interannual and longer timescales [Servain *et al.*, 1998]. It consists of 15 buoys moored from 38°W to 8°E and 19°S to 15°N that record sea temperature, salinity, at the surface and at several depths. The wind, the precipitations and the atmospheric pressure are also monitored. Adding CO<sub>2</sub> sensors on these moorings provide a good opportunity to record CO<sub>2</sub> as well as some parameters to help interpreting the data. A CO<sub>2</sub> sensor based on the CARIOCA technology [Bates *et al.*, 2000; Hood and Merlivat, 2001] has been installed on one of these moorings at 6°S, 10°W in the Gulf of Guinea. This new time-series station setup in the tropical Atlantic will provide high resolution time variability data over multi-months periods. For the first time it will allow us to document the diurnal to seasonal variability of fCO<sub>2</sub> in an undersampled region. On a longer timescale it will give insights into the behavior of the ocean under increasing atmospheric CO<sub>2</sub>. The purpose of this paper is to present

these new CO<sub>2</sub> data and to analyse the temporal variation of fCO<sub>2</sub> since the beginning of the monitoring in June 2006 until the end of 2006.

## 2. Methods

[6] The CO<sub>2</sub> sensor measures fCO<sub>2</sub> by the colorimetric method used on the CARIOCA drifting [Bakker *et al.*, 2001; Hood *et al.*, 1999, 2001] or moored buoys [Bates *et al.*, 2000; Copin-Montegut *et al.*, 2004] with an accuracy of  $\pm 3$   $\mu$ atm [e.g., Copin-Montegut *et al.*, 2004; Hood and Merlivat, 2001]. The sensor is calibrated against fCO<sub>2</sub> measurements made by an infrared detector. In order to setup the time-series in the tropical Atlantic, the CO<sub>2</sub> sensor had to be adapted to be installed on the PIRATA buoy itself. The sensor is located below the buoy at 1.5 m depth and the electronics is located on the platform about 1 m above sea level. A copper pipe has been used to supply seawater to the sensor in order to prevent biofouling. Copper reacts electrochemically with seawater and the oxidation reaction leads to a change of pH, hence a change of fCO<sub>2</sub>. However, the sensor is rinsed with 1 liter during 30 s so the exposure time of seawater with copper is very short and does not affect the fCO<sub>2</sub> measurements. The data are sent via Argos separately from the physical parameters of the PIRATA buoy. SEA-BIRD sensors record temperature at the surface, 20 m, 40 m, 60 m, 80 m, 120 m, 300 m, and 500 m. Salinity is measured at the surface, 20 m, 40 m, and 120 m. The buoy is also equipped with a rain gauge and an anemometer. Temperature, salinity, precipitations, wind speed are averaged daily and available on the PIRATA website (<http://www.pmel.noaa.gov/pirata>).

[7] Hourly fCO<sub>2</sub> and SST measurements are sent in real time. Data are also stored on the buoy to avoid any loss of data in case of transmission problems. The PIRATA buoys are usually serviced once a year so the sensor is designed to

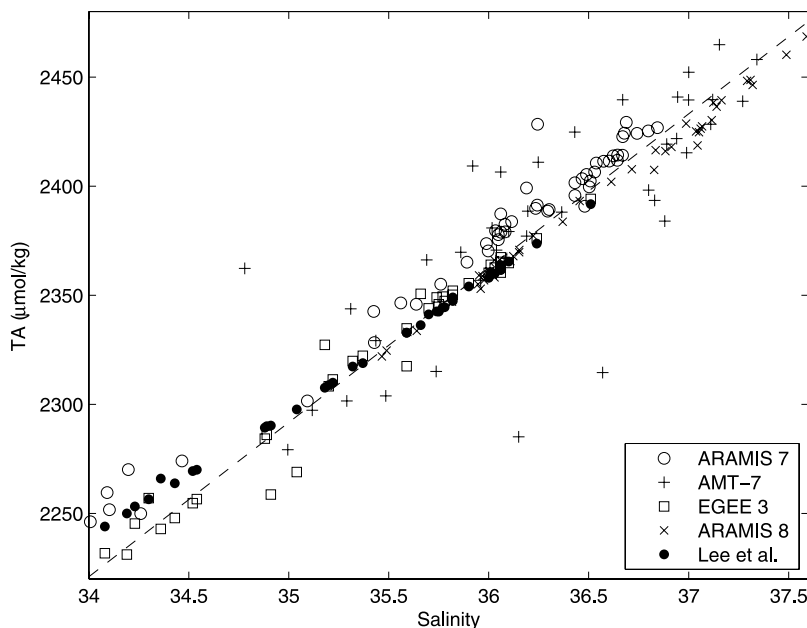


**Figure 2.** Alkalinity-salinity relationship (dashed line) determined from ARAMIS 7 and AMT-7 data and validated using ARAMIS 8 and EGEE 3 data between 20°S and 20°N. The *Lee et al.* [2006] relationship is shown with black circles.

work unattended for that length of time. The CO<sub>2</sub> sensor will be replaced each year in order to provide a continuous time series.

[8] As the CO<sub>2</sub> sensor has been installed during the EGEE 3 cruise, fCO<sub>2</sub> was also measured using an underway fCO<sub>2</sub> system consisting of a gas-seawater equilibrator and an infrared CO<sub>2</sub> gas analyzer, Licor 7000, which allows a comparison between the two systems. The precision of fCO<sub>2</sub> measurements is estimated to be  $\pm 1 \mu\text{atm}$ . After the buoy was moored at its location, the CO<sub>2</sub> sensor started to transmit its data. Several hours of measurements were made at this location before the ship moved further south along 10°W. The two systems give similar values of fCO<sub>2</sub> and SST (Figure 1).

[9] Alkalinity has been measured during ARAMIS cruises from France to Brazil. Alkalinity was also calculated during the AMT-7 cruise (UK-Uruguay) using DIC and fCO<sub>2</sub> measurements. Using these data between 20°S and 20°N, the following relationship between alkalinity and salinity (S in psu) is established, valid for the salinity range 34–37.5:

$$\text{TA} = 70.73(\pm 2.04)\text{S} - 183.82(\pm 73.5) \quad r^2 = 0.96 \quad (1)$$

[10] The standard error on the predicted alkalinity is  $\pm 11 \mu\text{mol/kg}$ . This relationship is robust and data from the ARAMIS 8 cruise (April 2006) validate the fit as well as the EGEE 3 data (Figure 2). The TA-S relationship is quite close to the relationship of *Rios et al.* [2005] who obtained a slope of  $63 \mu\text{mol kg}^{-1}/\text{psu}$  for the Azores area, and to the *Lee et al.* [2006] relationship. However, it is not valid for Congo waters as a salinity of zero would lead to a negative alkalinity. The salinity measured by the PIRATA buoy is available at daily resolution and is interpolated on an hourly basis, at the CO<sub>2</sub> data resolution. The salinity ranges from

35.6 to 36.3, which suggests that Congo waters do not reach this location. During the EGEE 3 cruise, the surface waters at this location were depleted in nutrients showing that nutrients brought by upwelled and Congo waters were consumed rapidly. From fCO<sub>2</sub> and salinity measurements, dissolved inorganic carbon (DIC) is calculated using the dissociation constants of *Mehrbach et al.* [1973] refitted by *Dickson and Millero* [1987]. An error of  $1 \mu\text{mol/kg}$  in alkalinity leads to an error of  $0.8 \mu\text{mol/kg}$  in DIC when DIC is calculated from fCO<sub>2</sub> and TA. As the error on the predicted alkalinity from salinity is  $11 \mu\text{mol/kg}$ , the resulting error on DIC is  $8.8 \mu\text{mol/kg}$ .

[11] The CO<sub>2</sub> flux (expressed in  $\text{mmol m}^{-2} \text{d}^{-1}$ ) is calculated using:

$$F_{\text{CO}_2} = k_{\text{CO}_2} \alpha (\text{fCO}_{2,\text{sea}} - \text{fCO}_{2,\text{atm}}) \quad (2)$$

where  $\alpha$  is the solubility of CO<sub>2</sub> [*Weiss, 1974*], fCO<sub>2,atm</sub> is the atmospheric fCO<sub>2</sub> measured during the EGEE 3 cruise (26 May–5 July 2006) and is equal to  $367.7 \pm 1.8 \mu\text{atm}$ . The gas exchange piston velocity for CO<sub>2</sub>,  $k_{\text{CO}_2}$ , for short-term winds, given by *Wanninkhof* [1992], is used. The daily wind speed available at the mooring, and measured at 4 m, is converted to a 10m wind speed and interpolated at hourly scale.

### 3. Oceanographic Conditions Near and at the Mooring

[12] The surface layer of the tropical Atlantic is occupied by the warm Tropical Surface Water (TSW), and underneath lies the South Atlantic Central Water [*Stramma and Schott, 1999*]. The mean circulation in the Gulf of Guinea is characterized by upwelling that brings cold and nutrient-and-carbon-rich water to the surface along the equator. This

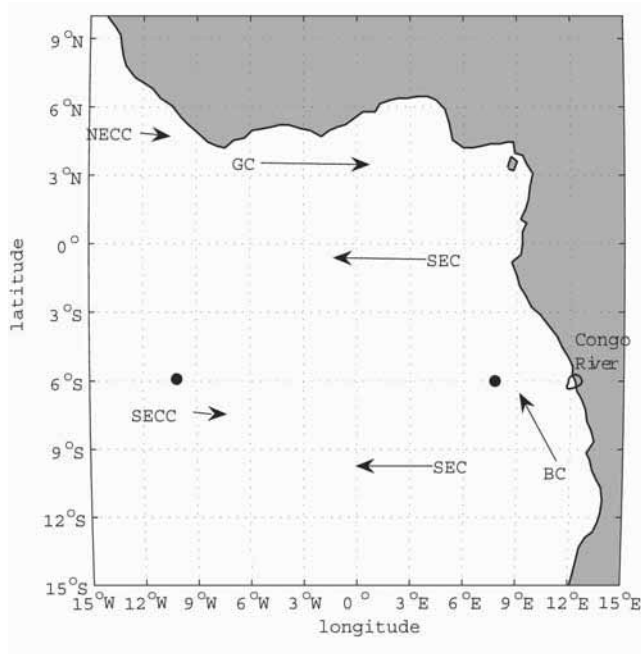


**Figure 3.** Surface circulation in the Gulf of Guinea showing the North Equatorial Counter Current (NECC), the South Equatorial Current (SEC) and the South Equatorial Counter Current (SECC). The Guinea current (GC) is an extension of the NECC current. The Benguela current (BC) is a coastal equatorward current. The locations of the PIRATA moorings at 6°S, 10°W and at 6°S, 8°E are also indicated (black circles). Only the mooring at 6°S, 10°W is equipped with a CO<sub>2</sub> sensor.

equatorial divergence occurs between about 0 to 4°S. The primary source of this upwelled water, salty and rich in O<sub>2</sub>, is the equatorial undercurrent (EUC), which flows eastward

across the basin [Gouriou and Reverdin, 1992]. The main surface current is the South Equatorial Current (SEC) that flows westward and extends from the surface to 100m. It is found between 4°N to 15–25°S depending on longitudinal location and the time of the year. Upwelled waters are transported by this current and their CO<sub>2</sub> concentration increases as the surface water warms up toward the west [Andrié *et al.*, 1986]. Molinari [1982] also observed an eastward current, the South Equatorial Countercurrent (SECC), flowing between 7°S and 9°S (Figure 3). It is formed near 30°W and is a recirculation of the southern branch of the SEC [Molinari, 1982]. It is characterized by warm and salty subtropical waters. This current is not very often mentioned as it is difficult to detect in maps of average surface velocity because it is subject to strong seasonal variations in flow directions. However, it was observed during the EGEE 3 cruise (B. Bourlès, personal communication).

[13] In addition to these large-scale currents, the Gulf of Guinea is affected by river discharge with the Congo (at 6°S), second world largest river, which supplies 40,600 m<sup>3</sup>/s of freshwater on annual average [Seyler *et al.*, 2003]. The highest flow occurs in December and in May but the extent of the Congo plume and its impact on the biogeochemical properties of the area are still largely unknown. However, low salinities seem to be restricted to a narrow coastal band [Piton and Kartavtseff, 1986] suggesting little offshore advection of the Congo River outflow. Since the 29th of June 2006, a new PIRATA buoy is moored at 6°S, 8°E (Figure 3) and should provide more insights on the Congo River outflow. From the beginning of the time series to the 4th of November 2006, the surface salinity has always been higher than 35 and from the 23rd of November the salinity was between 32.5 and 34.5 (PIRATA website). The surface salinity sensor did not provide any data since the 11th of December.

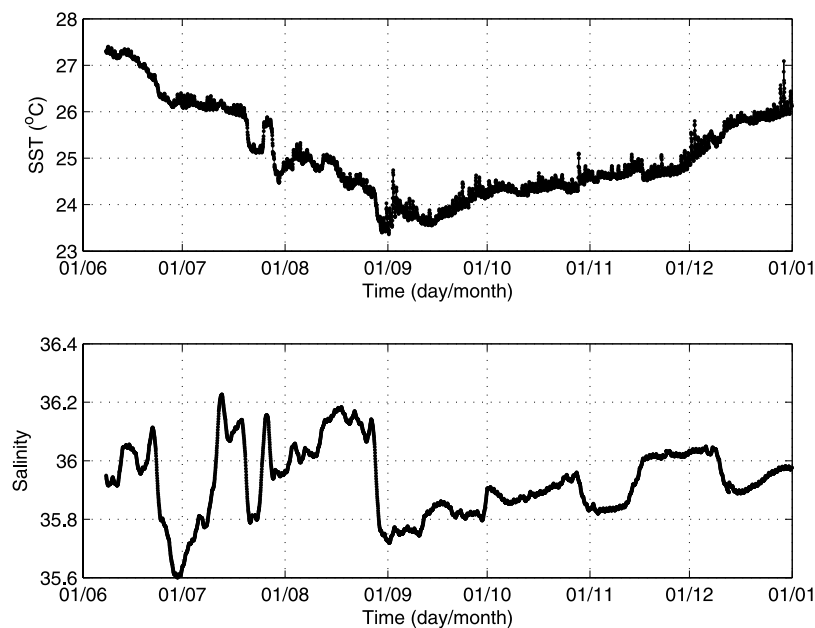


**Figure 4.** Distribution of temperature and salinity at 6°S, 10°W from 8th of June 2006 to 31 December 2006.

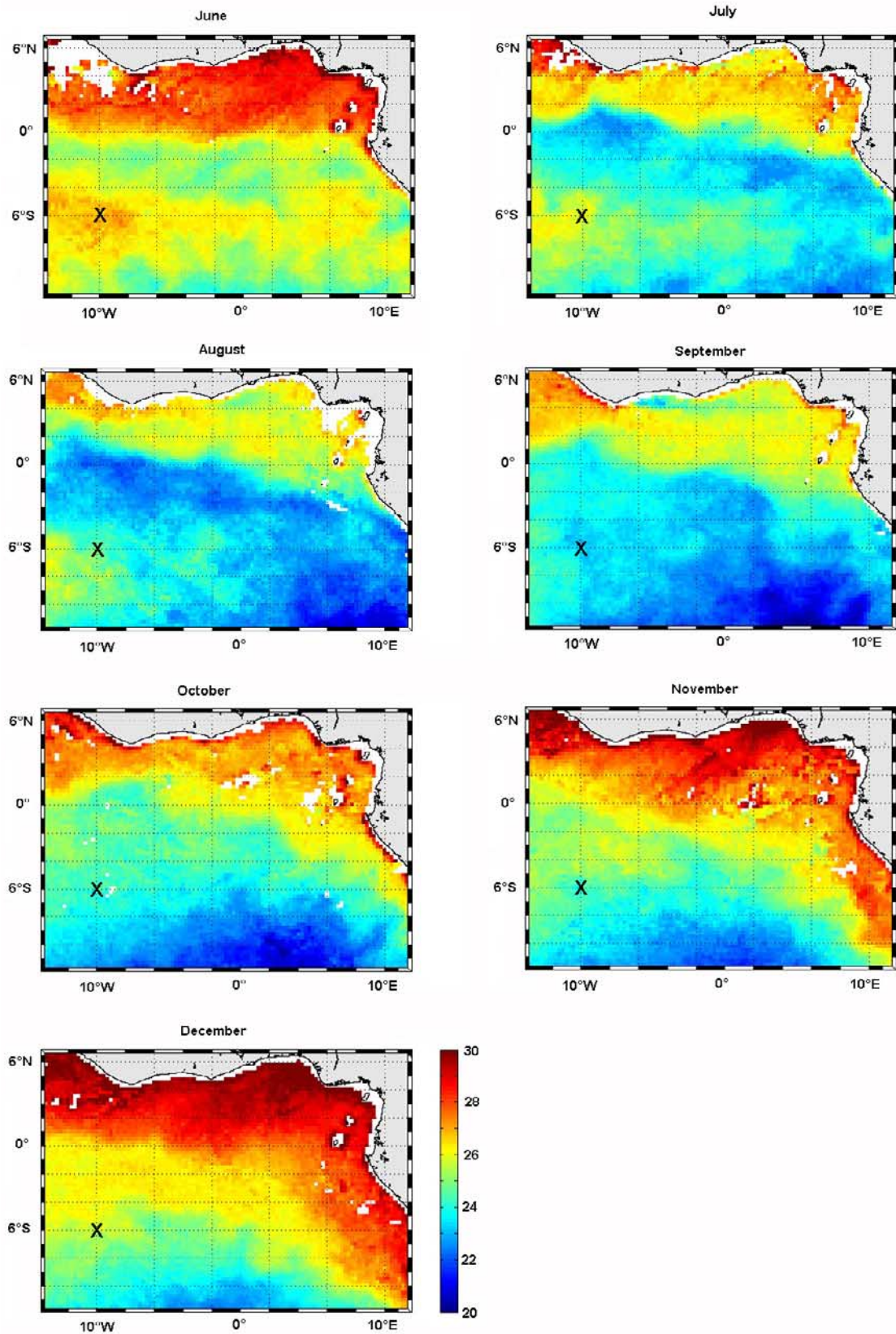


**Figure 5.** SST TMI imagery (9km resolution) of the Gulf of Guinea. The images are 3 days composites of 15 June, 15 July, 15 August, 15 September, 15 October, 15 November and 15 December 2006. The black cross corresponds to the location of the mooring.

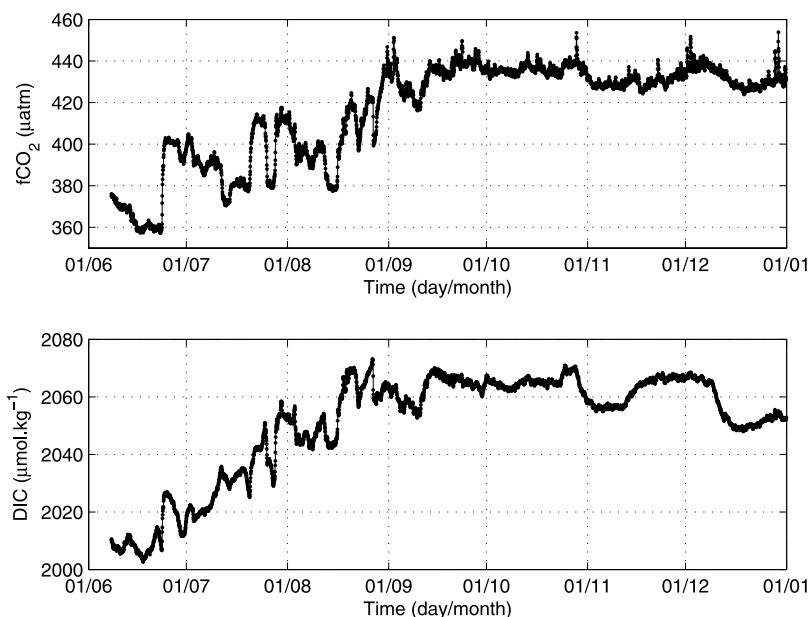


**Figure 6.** Distribution of fCO<sub>2</sub> and DIC at 6°S, 10°W from 8th June 2006 to the end of December 2006.

[14] At 6°S, 10°W, the buoy is located at the boundary between the westward SEC and the eastward SECC. During the main upwelling season (July to September) the wind comes from the Southeast. The lowest SST, around 23.5°C, is usually observed in August while the maximum SST, around 28.5°C, is reached in April so that the amplitude of the seasonal cycle is about 5°C at this site. From density data  $\sigma_{\theta}$  available from the PIRATA mooring the depth of the mixed layer can be calculated using a difference in  $\sigma_{\theta}$  of 0.125 kg m<sup>-3</sup> as a criterion. From June to September the mixed layer is constant at 40m suggesting that the mooring is not subject to local upwelling. However, it is affected by the advection of upwelled waters. The SST decreases throughout the upwelling season and the surface salinity can decrease to 35.6 (Figure 4). At this location, water with the salinity of 35.6 and temperature of 15°C is found at a depth of 120 m. Therefore as the surface temperature remains well above this value, this suggests that the water upwelled closer to the coast and was advected westward. This is confirmed by the satellite imagery of SST on which the spreading of the cold tongue can be seen with cold waters gradually invading the Gulf of Guinea from the south and joining the equatorial upwelling near 10°W, south of the equator, in July (Figure 5). The coldest SST are observed in August and September and from October, surface waters start warming up.

#### 4. Impact of the Upwelling on CO<sub>2</sub> Variations at 6°S, 10°W

[15] fCO<sub>2</sub> variations have been recorded since the 8th of June 2006. DIC is calculated using fCO<sub>2</sub> and the TA-S relationship. The fCO<sub>2</sub> and DIC distributions exhibit low values until the end of June followed by an increase until September and quite stable values afterward (Figure 6). At the beginning of the time-series, the sea surface temperature

is high with a value above 27°C and the water is close to equilibrium conditions with respect to atmospheric CO<sub>2</sub> as it is before the onset of the upwelling. This is consistent with the measurements made during the cruise where surface waters are slightly undersaturated with respect to atmospheric CO<sub>2</sub> on the 10°W section south of 5°S. The influence of the eastward SECC, warm and salty, flowing between 6°S and 9°S may explain the CO<sub>2</sub> undersaturations. Before the north-westward spreading of the cold tongue, two main water masses are present: warm and salty waters close to CO<sub>2</sub> equilibrium with the atmosphere, and colder and fresher waters rich in CO<sub>2</sub>. This is clearly seen during the EGEE 3 cruise when the ship moves from 10°S, 10°W to 5°S, 5°W. A sharp front occurs near 6.5°S showing the transition between tropical surface water (TSW) and upwelled water (Figure 7).

[16] The TSW is gradually replaced by the progression of the cold tongue and fCO<sub>2</sub> increases with values above 400 µatm, which is consistent with tropical upwelling values. For example, *Bakker et al.* [2001] reported similar values, in the equatorial upwelling, from their drifting buoy in 1997.

[17] Superimposed on the large scale feature of increasing fCO<sub>2</sub> associated with the spreading of upwelled waters, small SST and fCO<sub>2</sub> variations are recorded. Instead of having abrupt temperature and fCO<sub>2</sub> changes as those observed during the cruise, the fCO<sub>2</sub> and SST records are characterized by gradual variations. The SST decreases slowly from June to September and increases of 3°C over 4 months after September. (V-shape of the SST time-series, Figure 4). Within the decreasing trend of SST, peaks and troughs are observed. This pattern can be explained by the location of the mooring not being directly affected by coastal or equatorial upwellings. The spreading of the cold tongue mixes with TSW and generates meanders. Intrusions of tropical warm and salty water are associated with lower fCO<sub>2</sub> values and can be detected more easily once the

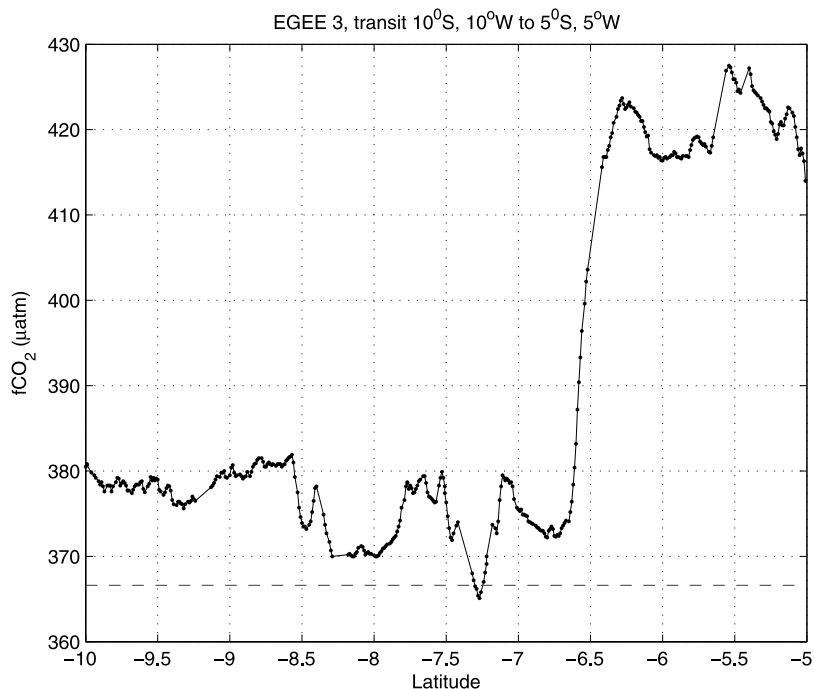


**Figure 7.** fCO<sub>2</sub> as a function of latitude from 10°S, 10°W to 5°S, 5°W during the EGEE 3 cruise. The dash line corresponds to the mean atmospheric value measured during the cruise.

signals are detrended, i.e., the linear trend is removed from the data, and normalized by dividing the detrended data by their standard deviation (Figure 8).

[18] From June to September the CO<sub>2</sub> variability is mainly driven by the development of the upwelling and strong correlations are observed between temperature, salinity and fCO<sub>2</sub>. Temperature and salinity are well correlated

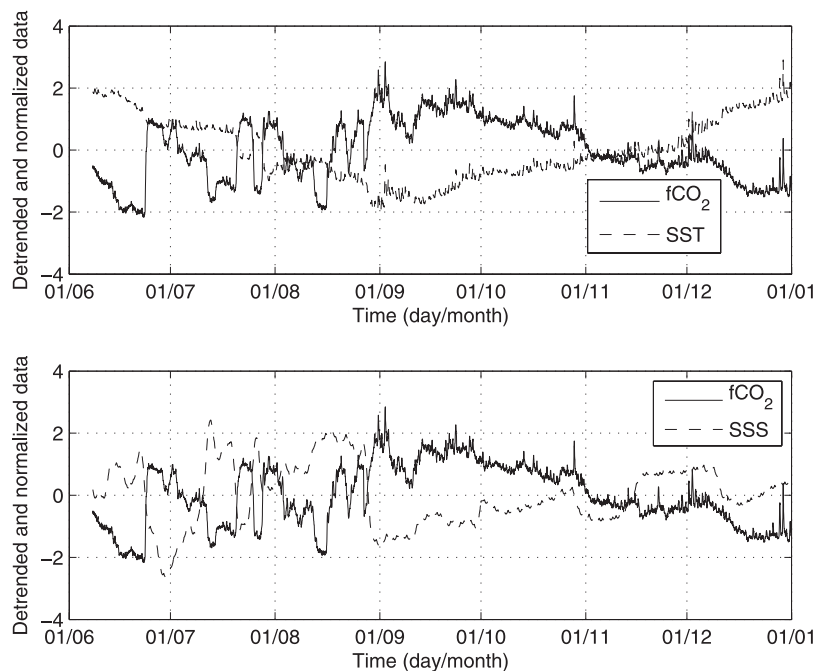


**Figure 8.** Detrended and normalized fCO<sub>2</sub> and SST as a function of time in day/month (top panel), detrended and normalized fCO<sub>2</sub> and SSS as a function of time (bottom panel). The detrended data are obtained by removing the linear trend. The detrended data are then divided by their standard deviation to normalize them.

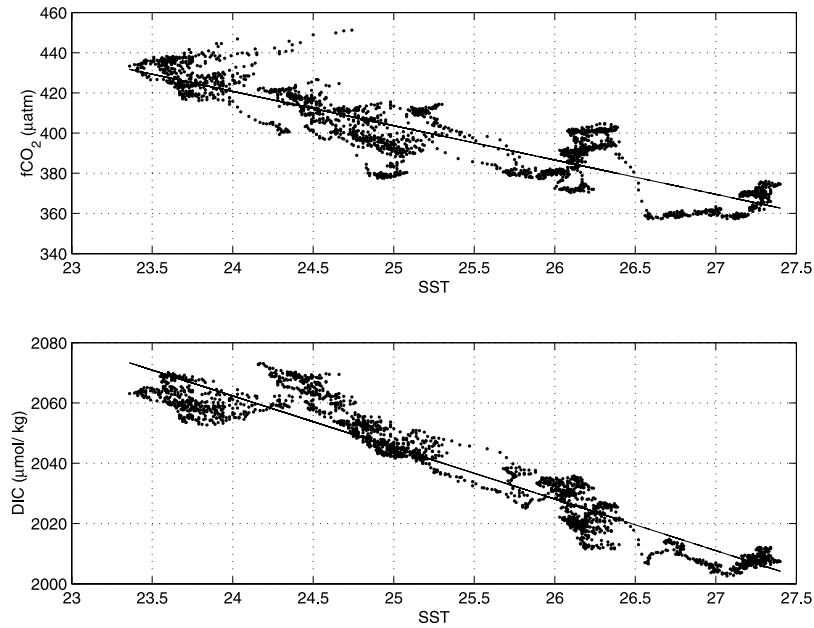


**Figure 9.** Relationships between fCO<sub>2</sub> and SST (top panel) and DIC and SST (bottom panel) between the 8th of June and the 15th of September 2006.

with warm and saltier waters corresponding to low CO<sub>2</sub> values, and with cold and fresher waters corresponding to upwelled waters rich in CO<sub>2</sub>. A relationship between fCO<sub>2</sub> and SST can be determined for the period 8 June to 15 September:

$$fCO_2 = -17.08 \cdot SST + 830.7 \quad \rho = -0.88 \quad (3)$$

A stronger relationship (correlation coefficient  $\rho = -0.95$ ) is found between DIC and SST:

$$DIC = -17.1 \cdot SST + 2473.1 \quad (4)$$

for the same period (Figure 9). The upwelling as well as convective mixing supply CO<sub>2</sub> rich waters to the surface so

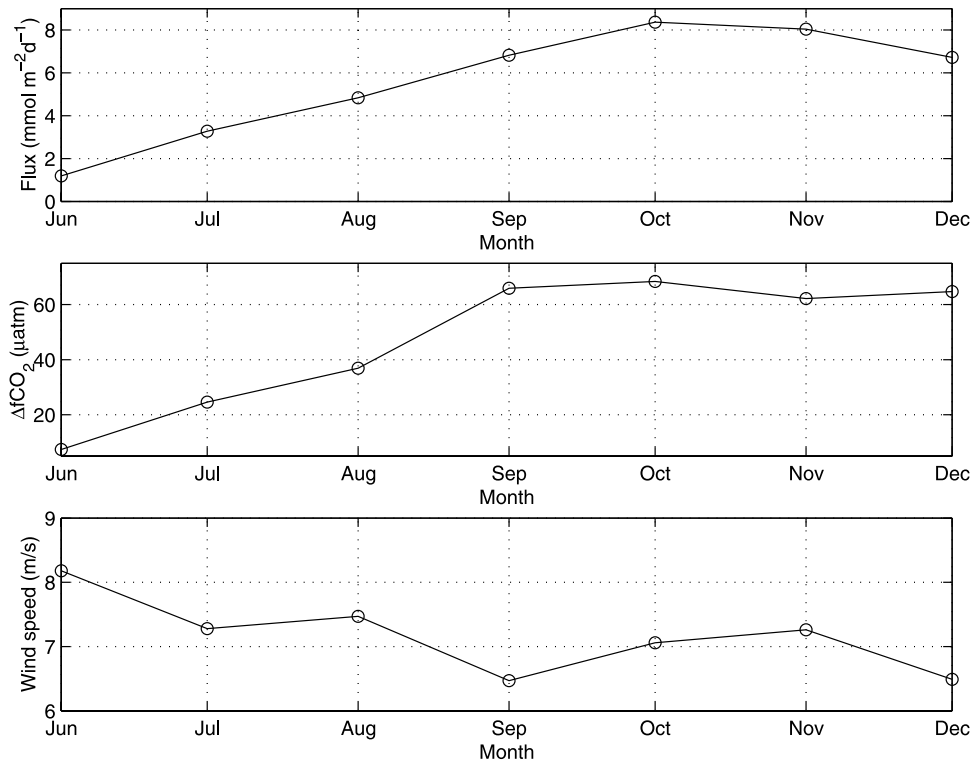


**Figure 10.** Monthly means of the CO<sub>2</sub> flux (top panel), ΔfCO<sub>2</sub> the difference of fugacity of CO<sub>2</sub> between the ocean and the atmosphere (middle panel) and the wind speed (bottom panel).



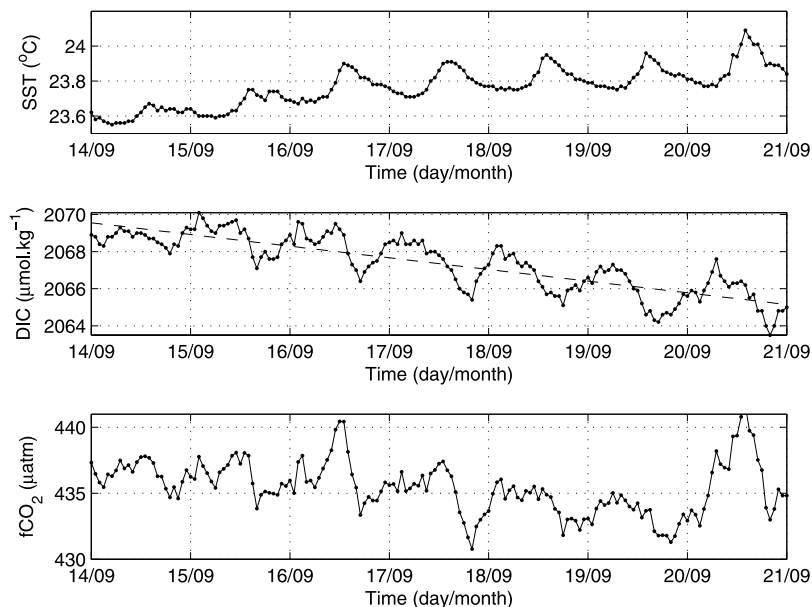


**Figure 11.** Diurnal cycles of SST, DIC and fCO<sub>2</sub> near the end of the upwelling season (14–20 September).

cold waters are associated with high CO<sub>2</sub> concentrations. The warming of surface waters increases the fugacity of CO<sub>2</sub> and results in high fCO<sub>2</sub> also associated with rather cold temperature around 24.5°C (Figure 9) so the fCO<sub>2</sub>-SST relationship is weaker than the DIC-SST one.

[19] After the upwelling season, i.e., from mid-September to December, no correlation between fCO<sub>2</sub> or DIC and SST can be determined. The temperature increases gradually from mid-September and is associated with a constant or slight decrease of fCO<sub>2</sub> (Figures 4 and 6). *Smethie et al.* [1985] and *Oudot et al.* [1987] noticed that warming during horizontal advection of surface water was also an important mechanism to explain high fCO<sub>2</sub> values. As the exchange with the atmosphere is a slow process there is no significant reduction of fCO<sub>2</sub> after the upwelling season. However, the lack of correlation with SST suggests that the solubility effect is not the only process responsible for the CO<sub>2</sub> variations. It might counterbalance the loss of CO<sub>2</sub> to the atmosphere and any biological uptake.

[20] *Oudot et al.* [1995] reported an annual CO<sub>2</sub> flux stronger during the upwelling season (July) than the warm season (January) from the FOCAL cruises. At 6°S, 10°W, the monthly CO<sub>2</sub> flux gradually increases from June (1.19 mmol m<sup>-2</sup> d<sup>-1</sup>) to September (6 mmol m<sup>-2</sup> d<sup>-1</sup>). A slight increase of wind speed leads to the maximum CO<sub>2</sub> flux in October (Figure 10). Nevertheless, the winds are quite steady, with an average at 7.3 m/s, and most of changes in the outgassing flux is attributed to changes in surface water fCO<sub>2</sub>. The warming of the surface waters helps to maintain high surface fCO<sub>2</sub> values so there is no significant reduction of the CO<sub>2</sub> flux from October to December.

## 5. Diurnal Variability

[21] The spreading of the cold tongue explains the high fCO<sub>2</sub> associated with cold temperatures. The changes from

non-upwelling to upwelling conditions are monotonic and the mixing between warm and cold waters account for the peaks and troughs noticed in the time-series. Superimposed on these variations, a diurnal cycle appears.

[22] During the development of the upwelling in June–July, the diurnal cycle is difficult to detect as two main water masses, the TSW and the cold tongue, are present. At the end of the upwelling, season, the diurnal cycle is detected for some short lengths of time, probably because of a relative homogeneity and stability of the surface waters. For example, from the 14th to 21st of September, SST increases from about 23.6°C to 24.1°C with amplitude of the diurnal cycle ranging from less than 0.1°C to 0.3°C. The diurnal variability of DIC ranges from less than 1 to about 3 μmol/kg and decreases of about 5 μmol/kg over the 7 day period (Figure 11). It is more difficult to detect the diurnal variability of fCO<sub>2</sub> because fCO<sub>2</sub> is subject to gas exchange and temperature variations so the correlation coefficient is only −0.13 compared to −0.78 for DIC and SST. For that reason fCO<sub>2</sub> at a given temperature is often used as a proxy for DIC.

[23] Fitting a linear regression to the DIC series leads to a slope of  $-0.63 \mu\text{mol kg}^{-1} \text{d}^{-1}$ . During the period considered (14–21 September) the mixed layer depth is constant at about 40 m so the total decrease of DIC over this period is  $\Delta\text{DIC} = -25.2 \text{ mmol m}^{-2} \text{d}^{-1}$ . The DIC variations are the result of changes due to loss of carbon to the atmosphere,  $\Delta\text{DIC}^a$ , vertical diffusion between the surface layer and upper layer of the thermocline,  $\Delta\text{DIC}^d$ , the net community production,  $\Delta\text{DIC}^b$ , and precipitation or dissolution of carbonate minerals,  $\Delta\text{DIC}^c$ :

$$\Delta\text{DIC} = \Delta\text{DIC}^a + \Delta\text{DIC}^d + \Delta\text{DIC}^b + \Delta\text{DIC}^c \quad (5)$$

[24] The loss of CO<sub>2</sub> to the atmosphere is calculated by the CO<sub>2</sub> flux across the air-sea interface. Over this period,

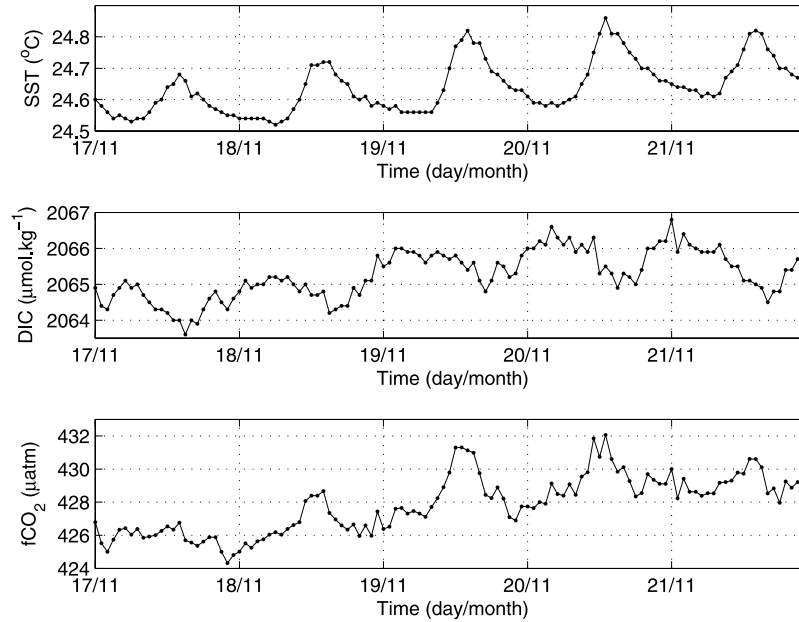


**Figure 12.** Diurnal cycles of SST, DIC and fCO<sub>2</sub> after the upwelling season (17–21 November).

the mean CO<sub>2</sub> flux is 8.49 mmol m<sup>-2</sup> d<sup>-1</sup>. The vertical diffusive flux is expressed by the Fick's law:

$$\Delta\text{DIC}^d = K_z \text{dC/dz} \quad (6)$$

where  $K_z$  is the vertical eddy diffusivity for the upper part of the thermocline,  $C$  the DIC concentration and  $z$  the depth.  $K_z$  is very low in tropical areas with strong stratification so we assume that this flux is negligible. *Denman and Gargett* [1983] gave an estimate of  $K_z$  of 4.1 m<sup>2</sup> s<sup>-1</sup>. The change of DIC due to precipitation or dissolution of carbonate minerals is expressed as a function of changes in alkalinity and DIC<sup>b</sup> [*Johnson et al.*, 1979] using the average stoichiometric composition of biogenic material P/N/C of 1/16/123 given by *Körtzinger et al.* [2001]:

$$\Delta\text{DIC}^c = 0.5(\Delta\text{TA} + 17/123 \Delta\text{DIC}^b) \quad (7)$$

[25] The net community production is obtained by difference between  $\Delta\text{DIC}$  and the other terms using equation (5) and is found equal to  $-17.8$  mmol m<sup>-2</sup> d<sup>-1</sup> (i.e., 211 mgC m<sup>-2</sup> d<sup>-1</sup>), which is a minimum estimate as we neglect the input of carbon from the subsurface layer. However, this estimate is consistent with previous estimates of primary production  $\sim 200$  mgC m<sup>-2</sup> d<sup>-1</sup> reported for typical tropical structures [*Pérez et al.*, 2005], so our assumption is reasonable. At 6°S, 10°W, the mixed layer is nitrate depleted, which characterizes a typical tropical structure [*Herbland and Voituriez*, 1979]. The biological activity is the dominant process responsible for the diurnal changes of DIC over the period 14–21 September. The CO<sub>2</sub> flux is quite significant as it is 48% of the biological DIC variation compared to the 9.5% reported by *Oudot* [1989] for the Guinea Dome area. This can be explained by the larger supersaturation observed at the mooring.

[26] Another period when the diurnal cycle is observed corresponds to a 5-day period in November. The fCO<sub>2</sub> cycle is more in phase with the SST (Figure 12) and the correlation between fCO<sub>2</sub> and SST is very strong ( $\rho = 0.80$ ) compared to  $-0.13$  for the previous series 14–21 September. Also, the DIC amplitude over the period is much smaller and increases by 0.29 μmol kg<sup>-1</sup> d<sup>-1</sup> showing no net carbon uptake over that period. fCO<sub>2</sub> expressed as a function of SST over that period gives:

$$\text{fCO}_2 = 17.00 \text{ SST} + 8.85 \quad (8)$$

[27] This corresponds to an increase of 4%/°C which means that the dominant process is the warming of the water mass. This process counterbalances the biological uptake on a daily basis on the fCO<sub>2</sub> signal: fCO<sub>2</sub> maxima are in phase with the SST maxima whereas DIC maxima correspond to SST minima. For this period, the diurnal variability in fCO<sub>2</sub> was primarily controlled by diurnal warming and cooling rather than net community production or gas exchange. This mechanism was also responsible for the fCO<sub>2</sub> diurnal variability observed in the Sargasso Sea [*Bates et al.*, 1998] and in the equatorial Pacific Ocean [*Goyet and Peltzer*, 1997].

## 6. Conclusions

[28] A new CO<sub>2</sub> time series station has been setup in the tropical Atlantic at 6°S, 10°W to provide high frequency data over multi months period. Hourly fCO<sub>2</sub> and SST data are transmitted by ARGOS. In addition to fCO<sub>2</sub> measurements, data from several cruises are used to determine an alkalinity- salinity relationship for the tropical Atlantic. The calculated alkalinity and the fCO<sub>2</sub> observations are then used to compute dissolved inorganic carbon. This relationship is quite robust so that, knowing salinity and fCO<sub>2</sub>, all the parameters of the carbon system can be determined.

[29] The main large scale features of the time series are characterized by a decrease of SST associated with an increase of fCO<sub>2</sub> corresponding to the upwelling that develops from the end of June to September. At the end of the upwelling season, SST increases and fCO<sub>2</sub> remains very high. The CO<sub>2</sub> flux gradually increases from June to reach a maximum of 8.37 mmol m<sup>-2</sup> d<sup>-1</sup> in October. Although the upwelling ends in September, the warming of the surface water maintains high fCO<sub>2</sub> values and explains that the strongest outgassing occurs in October. The upwelling signal observed at the mooring is not the result of vertical advection, as the mixed layer remains constant, but of the spreading of a cold tongue caused by the coastal upwelling.

[30] Diurnal variations are observed once the cold tongue has stopped its propagation. A simple DIC budget in the mixed layer shows that they can be explained by biological carbon fixation and solar heating. A net community production of 211 mg C m<sup>-2</sup> is estimated from this budget.

[31] Monitoring fCO<sub>2</sub> at this location will help in better understanding the temporal variability of fCO<sub>2</sub> and the key controlling processes governing the fCO<sub>2</sub> variability. On a longer timescale, the time series should provide some insights on the impacts of warm and cold years on the fCO<sub>2</sub> distribution.

[32] **Acknowledgments.** We thank Bernard Bourlès, of Institut de Recherche pour le Développement (IRD) Brest, for our participation in his EGEE/AMMA project and the crew members of the R/V *Atalante* for their help during the cruise. We are grateful to Nicolas Martin for sharing his programs to process the CO<sub>2</sub> ARGOS data. Data management for PIRATA moorings is conducted by the TAO project office at NOAA/PMEL in collaboration with many research institutes listed on the PIRATA website (<http://www.pmel.noaa.gov/pirata>). TMI data are produced by Remote Sensing Systems and sponsored by the NASA Earth Science and REASoN DISCOVER project. They are available at [www.remss.com](http://www.remss.com). We are grateful to Dominique Dagorne for retrieving satellite imagery. This work is funded by the European Integrated Project CARBOOCEAN (contract 511176-2), by the IRD, and the Centre National d'Etudes Spatiales (ARAMIS project). The manuscript benefited from the comments of two anonymous reviewers.

## References

- Ajao, E. A., and R. W. Houghton (1998), Coastal ocean of equatorial west Africa from 10°N to 10°S, in *The Sea*, edited by A. R. Robinson and K. H. Brink, pp. 605–631, John Wiley & Sons.
- Andrié, C., C. Oudot, C. Genthon, and L. Merlivat (1986), CO<sub>2</sub> fluxes in the tropical Atlantic during FOCAL cruises, *J. Geophys. Res.*, *91*(C10), 11,741–11,755.
- Bakker, D. C. E., J. Etcheto, J. Boutin, and L. Merlivat (2001), Variability of surface water fCO<sub>2</sub> during seasonal upwelling in the equatorial Atlantic Ocean as observed by a drifting buoy, *J. Geophys. Res.*, *106*(C5), 9241–9253.
- Bates, N. (2001), Interannual variability of oceanic CO<sub>2</sub> and biogeochemical properties in the Western North Atlantic subtropical gyre, *Deep Sea Res. II*, *48*, 1507–1528.
- Bates, N., T. Takahashi, D. Chipman, and A. H. Knap (1998), Variability of pCO<sub>2</sub> on diel to seasonal timescales in the Sargasso Sea near Bermuda, *J. Geophys. Res.*, *103*(C8), 15,567–15,585.
- Bates, N. R., L. Merlivat, L. Beaumont, and A. C. Pequignet (2000), Intercomparison of shipboard and moored CARIOCA buoy seawater fCO<sub>2</sub> measurements in the Sargasso Sea, *Mar. Chem.*, *72*(2–4), 239–255.
- Chavez, F. P., P. G. Strutton, G. E. Friederich, R. A. Feely, G. C. Feldman, D. C. Foley, and M. J. McPhaden (1999), Biological and chemical response of the equatorial Pacific Ocean to 1997–98 El Niño, *Science*, *286*(5447), 2126–2131.
- Copin-Montegut, C., M. Bégovic, and L. Merlivat (2004), Variability of the partial pressure of CO<sub>2</sub> on diel to annual time scales in the Northwestern Mediterranean Sea, *Mar. Chem.*, *85*, 169–189.
- DeGrandpre, M. D., T. R. Hammar, S. P. Smith, and F. L. Sayles (1995), In situ measurements of seawater pCO<sub>2</sub>, *Limnology and Oceanography*, *40*, 969–975.
- Denman, K. L., and A. E. Gargett (1983), Time and space scales of vertical mixing and advection of phytoplankton in the upper ocean, *Limnology and Oceanography*, *28*(5), 801–815.
- Dickson, A. G., and F. J. Millero (1987), A comparison of the equilibrium constants for the dissociation of carbonic acid in seawater media, *Deep Sea Res.*, *34*, 1733–1743.
- González Dávila, M., J. M. Santana Casiano, M. J. Rueda, O. Llinás, and E.-F. González-Dávila (2003), Seasonal and interannual variability of sea-surface carbon dioxide species at the European Station for Times Series in the Ocean at the Canary Islands (ESTOC) between 1996 and 2000, *Global Biogeochem. Cycles*, *17*(3), 1076, doi:10.1029/2002GB001993.
- Gouriau, Y., and G. Reverdin (1992), Isopycnal and diapycnal circulation of the upper equatorial Atlantic ocean in 1983–1984, *J. Geophys. Res.*, *97*(C3), 3543–3572.
- Goyet, C., and E. T. Peltzer (1997), Variation of CO<sub>2</sub> partial pressure in surface seawater in the equatorial Pacific Ocean, *Deep Sea Research*, *44*(9/10), 1611–1626.
- Hardman-Mountford, N. J., and J. M. McGlade (2003), Seasonal and interannual variability of oceanographic processes in the Gulf of Guinea: An investigation using AVHRR sea surface temperature data, *International Journal of Remote Sensing*, *24*(16), 3247–3268.
- Herbland, A., and B. Voituriez (1979), Hydrological structure analysis for estimating the primary production in the tropical Atlantic Ocean, *Journal of Marine Research*, *37*, 87–101.
- Hisard, P. (1980), Observation de réponses de type El Niño dans l'Atlantique tropical oriental Golfe de Guinée, *Oceanologica Acta*, *3*, 69–78.
- Hood, E. M., and L. Merlivat (2001), Annual to interannual variations of fCO<sub>2</sub> in the northwestern Mediterranean Sea: Results from hourly measurements made by CARIOCA buoys, 1995–1997, *Journal of Marine Research*, *59*(1), 113–131.
- Hood, E. M., L. Merlivat, and T. Johannessen (1999), Variations of fCO<sub>2</sub> and air-sea flux of CO<sub>2</sub> in the Greenland Sea gyre using high-frequency time series data from CARIOCA drift buoys, *J. Geophys. Res.*, *104*(C9), 20,571–20,584.
- Hood, E. M., R. Wanninkhof, and L. Merlivat (2001), Short timescale variations of fCO<sub>2</sub> in a North Atlantic warm-core eddy: Results from the Gas-Ex 98 carbon interface ocean atmosphere (CARIOCA) buoy data, *J. Geophys. Res.*, *106*(2; Sect 3), 2561–2572.
- Johnson, K. S., R. M. Pykowicz, and C. S. Wong (1979), Biological production and the exchange of oxygen and carbon dioxide across the sea surface in Stuart Channel, British Columbia, *Limnology and Oceanography*, *24*(3), 474–482.
- Körtzinger, A., J. I. Hedges, and P. D. Quay (2001), Redfield ratios revisited: Removing the biasing effect of anthropogenic CO<sub>2</sub>, *Limnology and Oceanography*, *46*(4), 964–970.
- Kuss, J., W. Roeder, K.-P. Wlost, and M. D. DeGrandpre (2006), Time-series of surface water CO<sub>2</sub> and oxygen measurements on a platform in the central Arkona Sea (Baltic Sea): Seasonality of uptake and release, *Mar. Chem.*, *101*, 220–232.
- Lee, K., L. T. Tong, F. J. Millero, C. Sabine, A. G. Dickson, A. G. Goyet, G.-H. Park, R. Wanninkhof, R. A. Feely, and R. M. Key (2006), Global relationships of total alkalinity with salinity and temperature in surface waters of the world's oceans, *Geophys. Res. Lett.*, *33*, L19605, doi:10.1029/2006GL027207.
- Mehrbach, C., C. H. Culbertson, J. E. Hawley, and R. M. Pykowicz (1973), Measurement of the apparent dissociation constants of carbonic acid in seawater at atmospheric pressure, *Limnology and Oceanography*, *18*, 897–907.
- Merle, J. (1980), Variabilité thermique annuelle et interannuelle de l'océan Atlantique équatorial Est. L'hypothèse d'un "El Niño" Atlantique, *Oceanologica Acta*, *3*(2), 209–220.
- Molinari, R. L. (1982), Observations of eastward currents in the tropical South Atlantic Ocean: 1978–1980, *J. Geophys. Res.*, *87*(C12), 9707–9714.
- Oudot, C. (1989), O<sub>2</sub> and CO<sub>2</sub> balances approach for estimating biological production in the mixed layer of the tropical Atlantic Ocean (Guinea Dome area), *Journal of Marine Research*, *47*, 385–409.
- Oudot, C., C. Andrié, and Y. Montel (1987), Evolution du CO<sub>2</sub> océanique et atmosphérique sur la période 1982–1984 dans l'Atlantique tropical, *Deep Sea Research*, *34*(7), 1107–1137.
- Oudot, C., J. F. Temon, and J. Lecomte (1995), Measurements of atmospheric and oceanic CO<sub>2</sub> in the tropical Atlantic: 10 years after the 1982–1984 FOCAL cruises, *Tellus*, *47B*, 70–85.
- Pérez, V., et al. (2005), Latitudinal distribution of microbial plankton abundance, production, and respiration in the Equatorial Atlantic in autumn 2000, *Deep-Sea Research I*, *52*, 861–880.
- Piton, B., and A. Kartavtseff (1986), Utilisation de bouées dérivantes à positionnement par satellite pour une meilleure connaissance de l'hydrologie de surface du golfe de Guinée., *Doc. Sci. Cent. ORSTOM de Brest*, *34*, 1–41.

- Rios, A., F. F. Pérez, M. Álvarez, L. Mintrop, M. González-Dávila, J. M. Santana Casiano, N. Lefèvre, and A. J. Watson (2005), Seasonal sea-surface carbon dioxide in the Azores area, *Mar. Chem.*, *96*, 35–51.
- Servain, J., A. J. Busalacchi, M. J. McPhaden, A. D. Moura, G. Reverdin, M. Vianna, and S. E. Zebiak (1998), A Pilot Research Moored Array In the Tropical Atlantic (PIRATA), *Bulletin- American Meteorological Society*, *79*(10), 2019–2032.
- Seyler, P., A. Coynel, P. Moreira-Turcq, H. Etcheber, C. Colas, D. Orange, J. P. Bricquet, A. Laraque, J. L. Guyot, and M. Meybeck (2003), *Organic carbon transported by the equatorial rivers: example of Zaire-Congo and Amazon Rivers*, Advances in Soil Science Editions, Ohio.
- Smethie, W. M., T. Takahashi, D. W. Chipman, and J. R. Ledwell (1985), Gas exchange and CO<sub>2</sub> flux in the tropical Atlantic Ocean determined from <sup>222</sup>Rn and pCO<sub>2</sub> measurements, *J. Geophys. Res.*, *90*, 7005–7022.
- Stramma, L., and F. Schott (1999), The mean flow field of the tropical Atlantic Ocean, *Deep Sea Res.*, *II*, *46*, 279–303.
- Wanninkhof, R. H. (1992), Relationship between wind speed and gas exchange over the ocean, *J. Geophys. Res.*, *97*(C5), 7373–7382.
- Weiss, R. F. (1974), CO<sub>2</sub> in water and seawater: The solubility of a non-ideal gas, *Mar. Chem.*, *2*, 203–215.
- Winn, C. D., Y. H. Li, F. T. Mackenzie, and D. M. Karl (1998), Rising surface ocean dissolved inorganic carbon at the Hawaii Ocean time-series site, *Mar. Chem.*, *60*(1–2), 33–47.
- 
- L. Beaumont and T. Danguy, DT INSU, 1 place Aristide Briand, 92195 Meudon, France.
- A. Guillot, DT INSU, Bâtiment Institut Polaire, BP 74, 29280 Plouzané, France.
- N. Lefèvre, IRD LOCEAN, Université Pierre et Marie Curie, 4 place Jussieu, 75252 Paris Cedex 05, France. (nathalie.lefevre@locean-ipsl.upmc.fr)